PROCEEDINGS OF THE ROYAL SOCIETY A MATHEMATICAL, PHYSICAL & ENGINEERING SCIENCES

The thermal diffusivity of silicon nitride/silicon carbide nanocomposites using a photothermal deflection technique

Aleksandra P. Chojnacka, C. Thomas Avedisian and Andreas Rendtel

Proc. R. Soc. Lond. A 1999 **455**, doi: 10.1098/rspa.1999.0427, published 8 August 1999

THE ROYAL SOCIETY

The thermal diffusivity of silicon nitride/silicon carbide nanocomposites using a photothermal deflection technique

By Aleksandra P. Chojnacka[1], C. Thomas Avedisian[1]† and Andreas Rendtel[2]

[1]*Sibley School of Mechanical and Aerospace Engineering, Cornell University, Ithaca, NY 14853, USA*
[2]*Arbeitsbereich Werkstoffphysik und-technologie, Technische Universitat Hamburg-Harburg, 21073 Hamburg, Germany*

Received 24 November 1997; accepted 24 August 1998

Measurements are presented to show the effect of mass fraction on thermal diffusivity of composites fabricated from 200 nm silicon carbide particles dispersed in a matrix of silicon nitride. The mean composite thermal diffusivity is measured over a mass fraction range of 0.05 to 0.30 using a photothermal deflection technique which creates a frequency-dependent thermal penetration depth in the material that can be used to reveal local inhomogeneities of thermal diffusivity. The results show that a maximum thermal diffusivity occurs at a mass fraction of 0.10. This peak value follows extrema in fracture toughness and creep rate at this particle loading that had been observed in prior studies of similarly fabricated nanocomposites. The results are discussed in terms of the competing influences of large thermal diffusivity of silicon carbide relative to silicon nitride, and the role of interfaces as volume fraction is changed due to the high surface-to-volume ratio of the nanosize particles. The measurements are compared with literature values and the trends are explained in terms of the differing particle sizes and binders used in the composites.

Keywords: mirage technique; ceramic nanocomposites; thermal conductivity; non-destructive evaluation; thermal contact resistance; tungsten–copper composite

1. Introduction

Silicon nitride (Si_3N_4) is an important material because of its high strength and resistance to creep, corrosion, oxidation and thermal shock (see, for example, Torti *et al*. 1973; Zdaniewski *et al*. 1979; Weiderhorn & Tighe 1983; Buljan *et al*. 1987; Suzuki 1987; Bhatt *et al*. 1990). The brittle nature and propensity to fracture of Si_3N_4 ceramics has motivated the search for composites consisting of Si_3N_4 as the matrix with an additive that mitigates these concerns. In particular, composites of silicon carbide (SiC) and Si_3N_4 have been proposed for improving fracture toughness (see, for example, Wei & Becher 1985; Shalek *et al*. 1986; Niihara *et al*. 1989). Tailoring an Si_3N_4 composite to achieve certain improvements in mechanical properties is complicated by the effect the additive and binder has on the thermal properties, the

† Author for correspondence.

most important of which is the thermal conductivity or thermal diffusivity which affect both the thermal stress in a material and energy management in a system.

Many prior studies of ceramic composites have focused on mechanical properties such as fracture toughness, strength and stiffness (see, for example, Evans 1995). Comparatively fewer studies have focused on the thermal conductivity and thermal diffusivity. While mechanical properties of composites can often be expressed as a weighted average of the two components (see, for example, Kelly 1996)—and the same is true for the thermal conductivity under certain conditions (Bigg 1986)—when the interface between particle and surrounding matrix influences heat flow in the composite the potential arises for interesting variations of thermal conductivity with volume fraction when the components have large differences in their thermal conductivity. SiC and Si_3N_4 is one such combination. The effect of volume fraction is further complicated by the necessity of using a binder for densification of the ceramic constituents. For a constant binder concentration, the binder can accumulate at the grain boundaries as the particle loading decreases and, therefore, play an increasingly important role in heat flow.

In this paper, we study the effect of mass fraction, Φ, of SiC on the thermal diffusivity of Si_3N_4/SiC nanocomposites at room temperature prepared using SiC particles of fixed mean size. The composites are prepared from SiC particles with an equivalent diameter of 200 nm. The large difference in thermal conductivity between pure Si_3N_4 and SiC (i.e. $\kappa_{SiC} \approx 270\ W\ m^{-1}\ K^{-1}$ and $\kappa_{Si_3N_4} \approx 30\ W\ m^{-1}\ K^{-1}$) when no binder is present in either material (Tummala & Rymaszewski 1989) coupled with the nanosize SiC particles used in the present study creates the potential for the particle–matrix interface to influence heat transfer in the composite as Φ is varied. An increase in the composite thermal conductivity with particle mass fraction could be argued on the basis of the much higher thermal conductivity of SiC compared with that of Si_3N_4. On the other hand, if the thermal conductivity decreases with increasing Φ, such a trend could be viewed as revealing the role of interfaces between SiC and Si_3N_4.

Several models for the thermal conductivity of composites have been developed which consider the thermal contact resistance between the filler particles and matrix. Some assume the filler particles to be spheres whose thermal fields may (Chiew & Glandt 1987) or may not (Hasselman & Johnson 1987) interact, or account for coated particles (Dunn & Taya 1993). The structural features of the composites examined here are far removed from the idealizations assumed in these models: spherical or cylindrical particles in a surrounding matrix with no binder present at the interface. However, these idealizations serve as a useful guide for understanding trends in the variation of particle concentration. Note that since $\rho_{SiC} \approx \rho_{Si_3N_4}$ then $\Phi \approx \phi$, where ϕ is the SiC volume fraction. The models reduce to the Maxwell (1873) equation for the thermal conductivity of a composite in the limit of 'low' volume fraction and negligible thermal contact resistance between particles and matrix:

$$\frac{\kappa_c}{\kappa_m} = \frac{1 + 2\beta\phi}{1 - \beta\phi}, \tag{1.1}$$

where

$$\beta = \left(\frac{\varepsilon - 1}{\varepsilon + 2}\right), \tag{1.2}$$

$\varepsilon \equiv \kappa_p/\kappa_m$ and $\beta < 1/\phi$. In equations (1.1) and (1.2), the ratio of thermal conductivities should be nearly the same as the ratio of thermal diffusivities since for bulk properties $(\rho C_p)_{SiC} \approx (\rho C_p)_{Si_3N_4}$ (Incropera & DeWitt 1990; Lide 1991). Thus, when we discuss trends in composite thermal diffusivity with volume fraction we expect them to be similar to thermal conductivity. From equation (1.1), the composite conductivity should vary monotonically with increasing Φ and show no extrema for constant β.

Prior measurements of thermal diffusivity of SiC/Si_3N_4 composites have shown differing trends which are believed to be due predominantly to variations of filler particle size and composition of the binder. Lange (1973) reports that the thermal diffusivity of Si_3N_4/SiC composites containing 5% (wt) MgO as a binder increases monotonically for $0 < \phi < 0.4$ and composites containing mean SiC particles size of 5 μm and 32 μm. These SiC particle sizes are large enough that heat flow in the composite is dominated by the higher thermal conductivity of the SiC filler and the effect of the thermal contact resistance between SiC particles and the surrounding Si_3N_4 matrix, where as the effect of the binder (with its lower thermal conductivity) is secondary, thus giving a result in line with equation (1.2). Hirano *et al.* (1995) investigated this same composite but used a different binder (as a mixture of 2% (wt) Al_2O_3 and 6% (wt) Y_2O_3 with the 8% (wt) binder concentration being held constant) and reduced the mean SiC particle size by factors of 50 and 320, to a mean size of less than 100 nm, thus producing an increase in interfacial area over the composites examined by Lange (1973) of approximately 10^3 and 10^5, respectively. A local minimum of thermal conductivity for $0.10 < \Phi < 0.20$ was measured. These prior results suggest that particle size and binder type can promote local extrema of thermal conductivity due to a controlling influence of interfaces. Indeed, the composites examined by Lange (1973) used particle radii larger than the Kapitza radius (estimated for the similar type of composites), which is considered to provide a measure for when interfaces can influence thermal diffusivity (Chung *et al.* 1997). The composites fabricated by Hirano *et al.* (1995) employed SiC particles below that Kapitza radius. Therefore, the thermal diffusivity of Hirano's composites is expected to be influenced by the particle–matrix interface.

Other (mechanical) properties of SiC/Si_3N_4 composites have also been found to exhibit extrema in the volume-fraction range $0.10 < \Phi < 0.20$. For example, Rendtel *et al.* (1997) measured a minimum creep rate and Sawaguchi *et al.* (1991) a maximum fracture toughness in this range. The connection between conductivity and such mechanical properties (see, for example, Gibiansky & Torquato 1996) further suggests that extrema in thermal conductivity are possible if observed in certain mechanical properties. In the present study we endeavoured to investigate the potential for thermal diffusivity to exhibit a maximum in the range $0 < \Phi < 0.30$. We chose an SiC particle size that was intermediate between those used by Lange (1973) and Hirano *et al.* (1995) where opposite trends of conductivity with volume fraction were measured. We fabricated composites with SiC particles of nominally 200 nm diameter using the hot-pressing method because this technique was used in prior studies that formed the motivation for the present investigation.

Measurements of thermal diffusivity are reported using the photothermal deflection (PD) technique (see, for example, Reyes 1988; Wei 1993; Chung 1995). The PD technique is in a class of laser-heating methods (see, for example, Graebner 1993) that creates a temperature distribution within a material by impingement of a laser

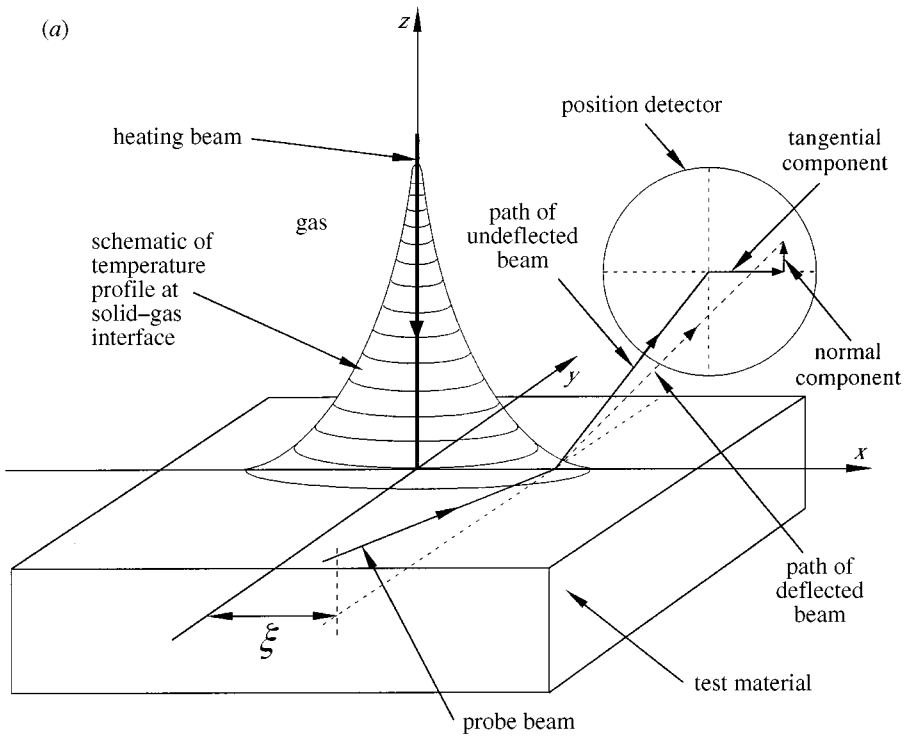

Figure 1. (*a*) Schematic of the photothermal deflection technique.

onto its free surface. A 'response variable' is then measured from which thermal diffusivity is inferred by matching the measurements with values predicted by a suitable theory for heat transfer in the material, rather like solving an inverse problem. The PD method has some advantages over other laser-based techniques that are attractive for application to composite materials in that it can measure a 'local' thermal diffusivity over a region of a material's surface, the extent of which is dependent on the modulation frequency of the heating laser beam. As with other transient heating techniques, the thermal diffusivity $\alpha \equiv \kappa/(\rho C_p)$, rather than the thermal conductivity, is measured. However, α is often the critical property in applications because the highest thermal stresses are generated during transient heating processes. Measurement of α can be used directly in analysis of time-dependent energy transport in engineering components.

2. Theory of the method

Figure 1*a* is a schematic diagram of the method for measuring α. A steady periodic temperature field is created in the test sample by heating a small spot on the surface with a modulated laser (the 'heating' beam) at a frequency f. A second laser beam (the 'probe' beam) bounces off the sample surface at a small shallow angle. The probe beam 'bends' in the vicinity of the heated spot because the index of refraction of air is locally reduced due to heat transfer from the heated spot through the solid and to the air above it. The 'response variable' mentioned in the previous section, from which the thermal diffusivity is obtained, is the bending of the probe beam, of which

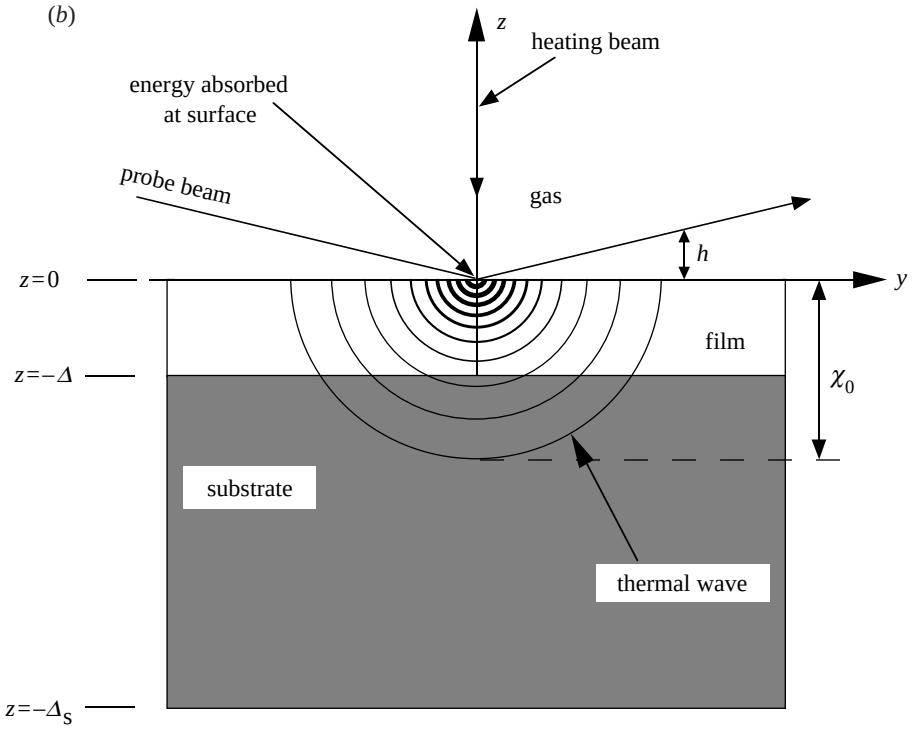

Figure 1. (*b*) Film-on-substrate geometry for PD showing the thermal wave.

there are two components, M_{norm} and $M_{\tan}$ (figure 1). An analytical development for the probe-beam deflection is then used to obtain thermal diffusivity by using the diffusivity as an adjustable parameter. One reason for modulating the heating beam is to facilitate an analytical development for heat transfer in the solid and air. For completeness we present here the main results of the theory used for analysing the experimental results reported in this paper.

The probe-beam components are related to the temperature gradient and index of refraction as

$$M_{\mathrm{norm}} = \frac{\mathrm{d}z}{\mathrm{d}y} = \frac{1}{n_0}\frac{\mathrm{d}n}{\mathrm{d}T}\int_{-\infty}^{\infty}\frac{\partial T}{\partial z}\,\mathrm{d}y = \frac{1}{n_0}\frac{\mathrm{d}n}{\mathrm{d}T}\frac{\partial \bar{\theta}_{\mathrm{g}}}{\partial z} \tag{2.1 a}$$

and

$$M_{\tan} = \frac{\mathrm{d}x}{\mathrm{d}y} = \frac{1}{n_0}\frac{\mathrm{d}n}{\mathrm{d}T}\int_{-\infty}^{\infty}\frac{\partial T}{\partial x}\,\mathrm{d}y = \frac{1}{n_0}\frac{\mathrm{d}n}{\mathrm{d}T}\frac{\partial \bar{\theta}_{\mathrm{g}}}{\partial x}, \tag{2.1 b}$$

where $\bar{\theta}_j$ (j = g, f, or s to denote the gas, film or substrate, respectively) is a complex temperature defined as

$$\bar{\theta}_j = \int_{-\infty}^{\infty}\theta_{0j}(x,y,z)\,\mathrm{d}y,$$

and θ_{0j} is the amplitude of the thermal wave resulting from the periodic heat source, i.e. $\theta_j = \theta_{0j}\exp(-2\pi f t\mathrm{i})$ and $\theta_j = \Delta T_j - \mathrm{i}\Delta T_j^*$, where $\mathrm{i} = \sqrt{(-1)}$. $\bar{\theta}_j$ is determined

by solving a multidomain transient conduction problem using the appropriate energy equations. $\Delta T_j = T_j - T_i$ (j = s, g and f for substrate, gas, and film, respectively), where T_i is the temperature far from the heating source. The ΔT_j are employed in the boundary conditions at $z = 0$ (gas–film interface) and $z = -\Delta$ (film–substrate interface). ΔT_j^* are determined according to the method of complex combination (Arpaci 1966). The general material system analysed consists of a thin film (f) of thickness Δ on a semi-infinite substrate (s) of thickness $\Delta_s - \Delta$ as shown in figure 1*b*. For the bulk semi-infinite composites we studied here, $\Delta = 0$ and $\Delta_s \to \infty$. The shading shown in figure 1*b* depicts the extent of penetration of the thermal wave that emanates from the heated spot ($x = z = 0$). The penetration depth χ_0 is discussed later.

The following assumptions are used to model the temperature field in the solid: (1) heat transfer in the gas is via conduction only (convection and radiation are neglected); (2) the solid is isotropic; (3) thermal contact resistance between the film and substrate is neglected; and (4) properties are independent of temperature. Additionally, it is important to discuss the nature of absorption of the heating-beam power in the test sample. We present below formulations which assume that the heating beam is absorbed in a small point-like volume at the surface. Salazar *et al.* (1989) extended this assumption to consider absorption in a material that follows an exponential decay law. The question of convection losses is discussed in § 5. Extension of the analysis to orthotropic materials is a subject of on-going work (Nguyen & Avedisian 1994). The composites we fabricated are isotropic, based on microstructural observations using SEM.

Considering conduction in both the solid and gas phases, assuming a steady periodic heat source at the gas–solid boundary and $\Delta_s \to \infty$, leads to solutions for the temperature field in the respective domains (substrate, film and gas) as

$$\bar{\theta}_g = -\frac{1}{2\pi}\int_{-\infty}^{\infty} \frac{\exp(\mathrm{i}kx - \zeta_g z)}{\kappa_f \zeta_f \coth(\phi_s) + \kappa_g \zeta_g}\,\mathrm{d}k, \tag{2.2a}$$

$$\bar{\theta}_f = -\frac{1}{2\pi}\int_{-\infty}^{\infty} \frac{\sinh(\phi_s + \zeta_f z)\mathrm{e}^{\mathrm{i}kx}}{\kappa_f \zeta_f \cosh(\phi_s) + \kappa_g \zeta_g \sinh(\phi_s)}\,\mathrm{d}k, \tag{2.2b}$$

$$\bar{\theta}_s = -\frac{1}{2\pi}\int_{-\infty}^{\infty} \frac{\sinh(\phi_s - \zeta_f \Delta)\exp(\mathrm{i}kx + \zeta_s(z + \Delta))}{\kappa_f \zeta_f \cosh(\phi_s) + \kappa_g \zeta_g \sinh(\phi_s)}\,\mathrm{d}k, \tag{2.2c}$$

where ϕ_s is given by

$$\phi_s = \zeta_f \Delta + \tanh^{-1}\left(\frac{\kappa_f \zeta_f}{\kappa_s \zeta_s}\right) \tag{2.3a}$$

and

$$\zeta_j = \sqrt{k^2 - \frac{\mathrm{i}2\pi f}{\alpha_j}}, \quad \text{where } \mathrm{Re}(\zeta_j) > 0 \tag{2.3b}$$

(j = g, f or s for gas, film, and substrate, respectively).

Explicit expressions for the beam-bending components are obtained by substituting equation (2.2*a*) into equations (2.1) and accounting for the heating and probe

beams:

$$M_{\text{norm}} = -\frac{1}{2\pi}\frac{1}{n_0}\frac{\mathrm{d}n}{\mathrm{d}t}\int_{-\infty}^{\infty}\frac{\zeta_{\mathrm{g}}\exp(\mathrm{i}kx - k^2(\frac{1}{4}R_1^2+\frac{1}{4}R_2^2) - (h^2/R_2^2))}{\kappa_{\mathrm{f}}\zeta_{\mathrm{f}}\coth(\phi_{\mathrm{s}}) + \kappa_{\mathrm{g}}\zeta_{\mathrm{g}}}(\mathrm{erfw}(z_2) - \mathrm{erfw}(z_1))\,\mathrm{d}k, \tag{2.4}$$

$$M_{\tan} = \frac{1}{2\pi}\frac{\mathrm{i}}{n_0}\frac{\mathrm{d}n}{\mathrm{d}t}\int_{-\infty}^{\infty}\frac{k\exp(\mathrm{i}kx - k^2(\frac{1}{4}R_1^2+\frac{1}{4}R_2^2) - (h^2/R_2^2))}{\kappa_{\mathrm{f}}\zeta_{\mathrm{f}}\coth(\phi_{\mathrm{s}}) + \kappa_{\mathrm{g}}\zeta_{\mathrm{g}}}(\mathrm{erfw}(z_2) + \mathrm{erfw}(z_1))\,\mathrm{d}k, \tag{2.5}$$

where

$$z_{1,2} = \tfrac{1}{2}\zeta_{\mathrm{g}}R_2 \mp (h/R_2) \tag{2.6}$$

and $\mathrm{erfw}(z) \equiv \mathrm{e}^{z^2}\,\mathrm{erfc}(z)$. In equation (2.6), if the probe beam bounces before the heated spot, '−' is used for z_1 and '+' for z_2; and conversely if the probe beam bounces after the heated spot (Chung 1995).

As stated in § 1, an advantage of the PD technique is that it allows local probing of regions of the material by varying the modulation frequency of the heating beam. The penetration depth for a steady periodic heat source over the surface of a semi-infinite solid is equal to $[\alpha/(\pi f)]^{1/2}$. The problem of interest here is slightly different in that surface heating occurs over a localized zone of radius R_1. For this case a suitably defined penetration depth for the spot-heating case, χ_0 (figure 1*b*), is expected such that $\chi_0 \propto f^{-1/2}$.

At high frequencies (or low α), and taking Δ_{s} as the relevant length-scale, a thermally thick or essentially semi-infinite material will correspond to $\Delta_{\mathrm{s}} > \chi_0$—a condition which can be forced by high-frequency heating. In practice, measurement difficulties arise for heating at high frequencies because the amount the probe beam bends decreases as frequency increases, which decreases the signal-to-noise ratio.

We are interested in applying equations (2.4) and (2.5) to 'bulk' materials because the data analysis is considerably simplified for this case; their application to thin films has been recently demonstrated (Wei *et al*. 1995). A bulk material can be viewed in two ways with regard to figure 1*b*: $\Delta \to \infty$ and the 'film' becomes the material of interest, or $\Delta \to 0$ and the substrate of thickness Δ_{s} is the material of interest. Both limits in equations (2.4) and (2.5) yield the same temperature field for a periodic heat source (Reyes 1988). Since $\Delta = 0$ for our materials, frequencies were selected to ensure that $\Delta_{\mathrm{s}} > \chi_0$, where $\Delta_{\mathrm{s}} \approx 4.0$ mm for the specimens we fabricated, as discussed in § 4.

When $\Delta_{\mathrm{s}} > \chi_0$ for monolithic materials, the real part of the tangential beam deflection from equation (2.5), $\mathrm{Re}(M_{\tan})$, can be shown (by plotting $\mathrm{Re}(M_{\tan})$ values numerically generated from equation (2.5) with x) to have a first non-central zero (which we will take as χ_0 for reasons discussed in § 5) that varies linearly with $f^{-1/2}$:

$$\chi_0 = c + (m/f^{1/2}). \tag{2.7}$$

Furthermore, the slope m in equation (2.7) was found (Reyes *et al.* 1987) to be related to thermal diffusivity, α, as

$$m = b\sqrt{\pi\alpha}. \tag{2.8}$$

In equation (2.8) b is a constant (independent of α) that is evaluated by determining χ_0 from the variation of $\mathrm{Re}(M_{\tan})$ with x using equation (2.5). When $h = 0$ and a semi-infinite solid is assumed, the numerical procedure gives $b \approx 1.2$. It is emphasized that this value is the result of assuming total absorption of the heating beam at the test-material surface. Salazar *et al.* (1989) extended this analysis to the case of volumetric absorption of the heating beam for a material that obeys an exponential absorption law. For this case, b in equation (2.8) will depend on the absorption coefficient of the composite. As a result, α would depend on composition not only through the relationship between m and ϕ but also through the variation of b with ϕ for a material that absorbs volumetrically. The absorption coefficient must be known for each composition to determine the appropriate value of b.

Figure 2*a* shows a typical result of how $\mathrm{Re}(M_{\tan})$ varies with $\mathrm{Im}(M_{\tan})$, with the particular conditions being for a $\Phi = 0.15$ SiC composite at a frequency of 2000 Hz. These data are direct outputs from the lock-in amplifier. Each point on this figure was obtained at a different offset distance x. A cross-plot of $\mathrm{Re}(M_{\tan})$ from data like those shown in figure 2 with x then determines the aforementioned 'root', χ_0, which when plotted against $f^{-1/2}$ gives m from equation (2.8) (see § 5 for more details). In reality, $h \neq 0$. A recommendation is discussed by Salazar *et al.* (1991) to correct the measurements. It involves 'rotating' the variation of $\mathrm{Re}(M_{\tan})$ with $\mathrm{Im}(M_{\tan})$ until the longest flat side of the 'double loop' shown in figure 2*a* becomes parallel with the real axis (figure 2*b*). A cross-plot of the 'adjusted' $\mathrm{Re}(M_{\tan})$ values that result from this rotation is then used to obtain χ_0. When this rotation is done, better agreement is obtained between measured and predicted thermal diffusivity values when using equations (2.7) and (2.8) and a b value obtained from the $h = 0$ analysis (i.e. $b \approx 1.2$).

3. Experimental arrangement

Figure 3 is a schematic diagram of the experimental arrangement. The main components are the following: the heating beam (an Innova 70 (5 W) argon–ion laser); the probe beam (a Uniphase U-130-P helium–neon laser); and a position detector for measuring deflection of the probe beam. Modulation of the heating beam is done by an acousto-optic (AO) modulator. The measured heating-beam radius at the impingement point is *ca.* 13 μm and the probe-beam radius at the surface is *ca.* 10 μm for the present set-up. The heating-beam power was fixed at 30 mW for the experiments reported here. The materials examined are absorbing at the heating-beam wavelength (514 nm).

An experiment proceeds by first aligning the waste of the probe and heating beams by an automated process. The heating beam is stepped in small increments along the y-direction (figure 1). For each y the heating beam is scanned across the sample in the x-direction in increments of 1–5 μm and the normal component of the probe-beam deflection is recorded. The profile of a normal deflection versus x is Gaussian-like. The procedure is continued until a peak of this profile reaches a maximum for some location y. Similarly, the focal point of the heating beam is searched by moving the focal lens in the z-direction. The final aligned position is $x = y = z = 0$ in figure 1.

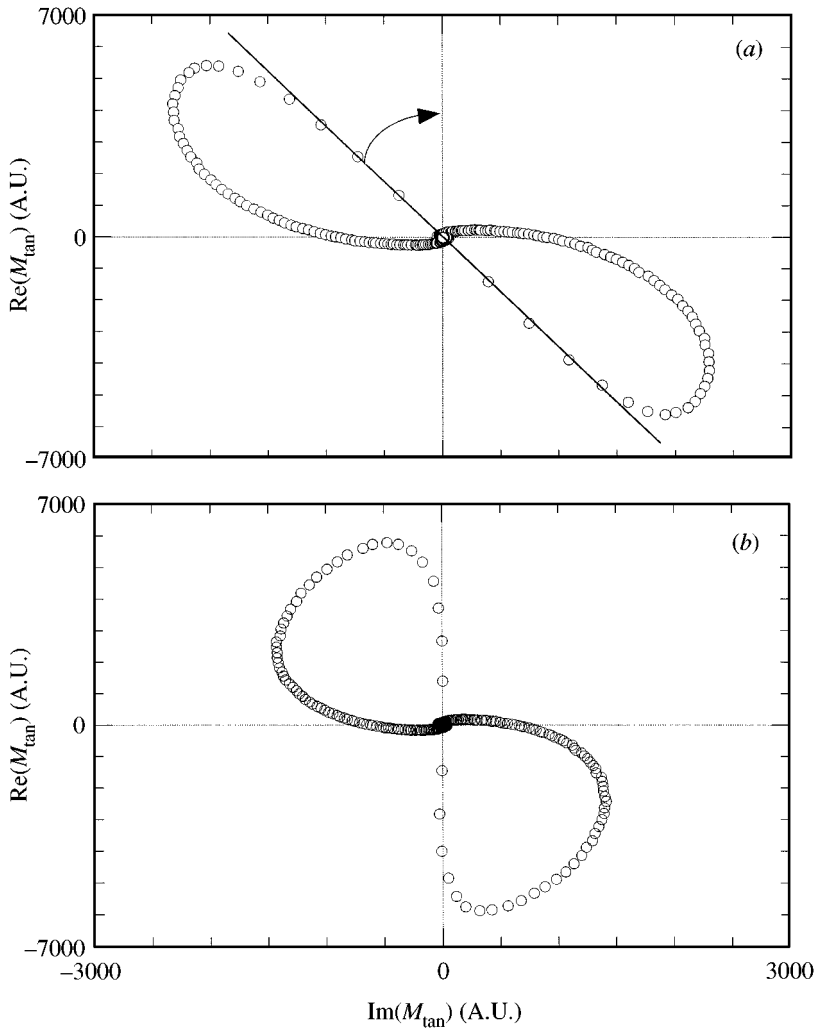

Figure 2. Variation of $\mathrm{Re}(M_{\tan})$ with $\mathrm{Im}(M_{\tan})$ for 15 wt % SiC at a frequency of 2000 Hz: (*a*) raw data before rotation; (*b*) data after rotation.

All of the data reported here were obtained by bouncing the beam because of the increased signal-to-noise ratio that results. The composite surface had to be polished to allow for specular reflection of the probe beam.

The heating beam is scanned across the sample in the x-direction (figure 1) in increments of 1 μm while holding the modulation frequency constant. Typically, $-0.5\ \mathrm{mm} < x < 0.5\ \mathrm{mm}$ for the data analysed. Outside this range, we found probe-beam deflections to be very small for the Si_3N_4/SiC composites. At each position, x, the tangential beam deflection components (real and imaginary parts) are stored by a lock-in amplifier (EG&G Princeton Applied Research model 5302) and subsequently transported to a PC-based data acquisition system. The lock-in reduces signal noise from the position sensor circuit (modulation frequencies equal to multiples of 60 Hz are avoided). Typical frequencies range from 10 Hz to 10 000 Hz.

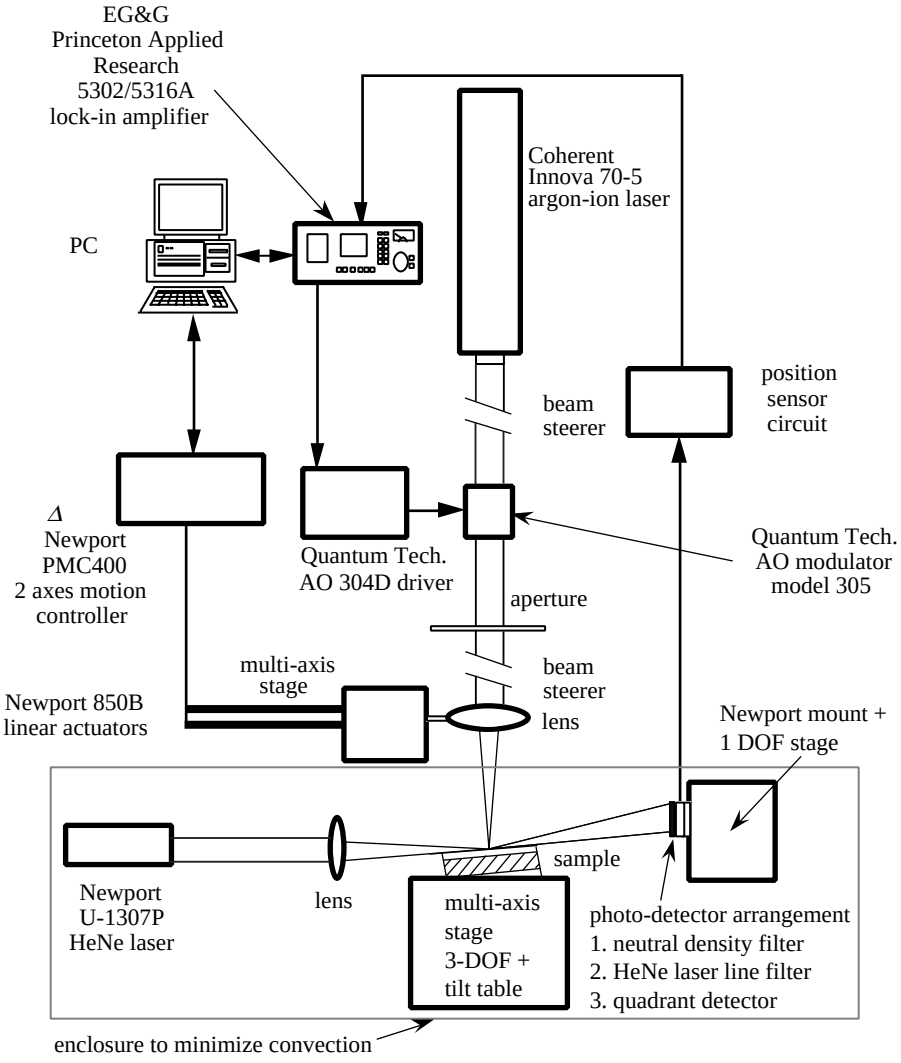

Figure 3. Experimental arrangement for PD.

4. Fabrication of materials

The Si_3N_4/SiC nanocomposites were prepared by conventional hot-pressing (HP). The starting material was a high-purity α-Si_3N_4 powder (E10, Ube Industries Ltd, Japan), transformed to β-Si_3N_4 during hot-pressing, which was mixed with an experimental SiCN powder prepared by a plasma-spray technique (Palchevskis *et al*. 1993) containing 80 wt % SiC. The sintering aid was Y_2O_3 ('fine' grade from H. C. Starck Co., Germany). The HP temperature was 1800 °C. Processed materials consist of β-Si_3N_4, α-SiC (polytypes 4H, 6H, and 33R), $Y_2Si_3N_40_3$, and a minor amount of amorphous YSiON glass. All materials were fabricated at the Fraunhofer Institute of Ceramic Technologies and Sintered Materials in Dresden, Germany. Further details

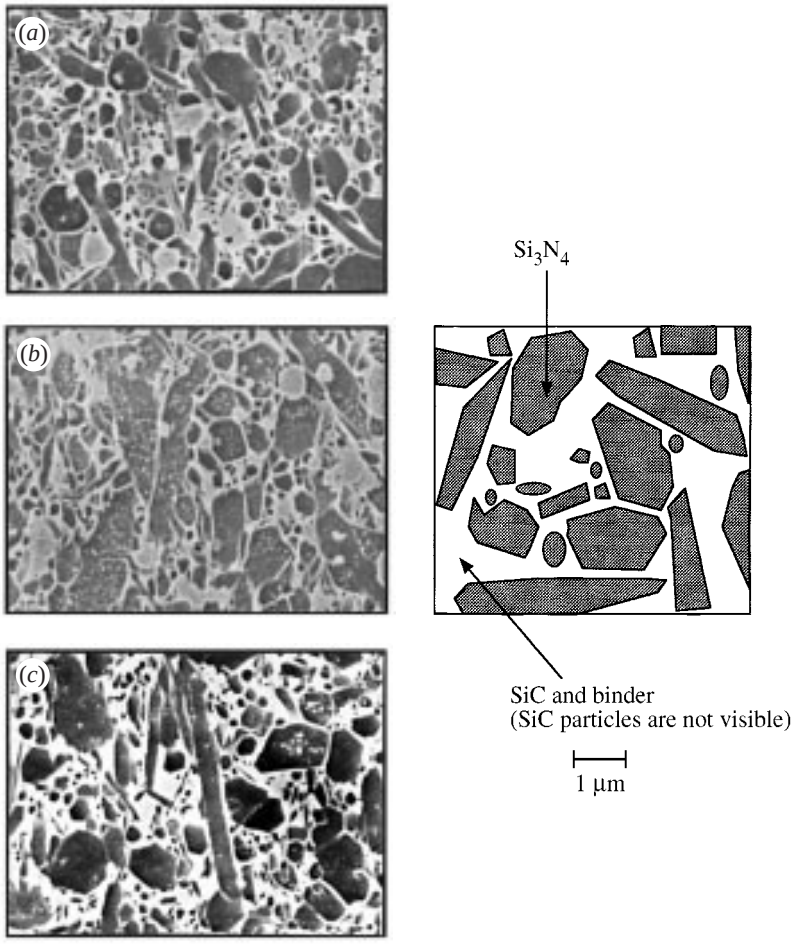

Figure 4. SEM micrographs of SiC/Si_3N_4 composites containing: (*a*) $\Phi = 0.05$; (*b*) $\Phi = 0.10$; (*c*) $\Phi = 0.15$ of SiC.

of the fabrication technique are described in Herrmann *et al*. (1993, 1997), Hermel *et al*. (1994) and Rendtel *et al*. (1997).

We fabricated composites into 80 mm diameter disks, 6–7 mm thick. The samples were machined into rectangular blocks (10 mm wide, 10 mm long, 4 mm high) by cutting and grinding with diamond tools. One millimetre was ground away from the hot-pressed surface. Final grinding on all sides was performed using a 320 grit diamond wheel. The surface used for the measurement of the thermal diffusivity was polished using 1 μm diamond paste, which resulted in a smooth (mirror-like) surface.

SEM photographs were taken on polished and plasmachemically etched sections at 10 000× magnification. Figure 4 shows SEM photographs for SiC mass fractions of 0.05, 0.10 and 0.15. Plasma etches only the Si_3N_4 grains and leaves intact the SiC and binder. A canal-like structure results that is boarded by SiC and binder to promote contrast between the SiC–binder edge and Si_3N_4 grains. The Si_3N_4 are the darker areas and the SiC particles and the binder phase are the brighter areas. Since there is no contrast between binder and individual SiC particles, SiC particles are

not visible. The micrographs show that the overall microstructure of the samples is similar and that there are no microstructural features of the $\Phi = 0.10$ sample that would forecast unusual behaviour of energy transport at this composition.

Quantitative determination of grain and particle sizes was carried out on a number of SEM pictures. The materials have elongated Si_3N_4 grains with an equivalent grain diameter of *ca.* 120 nm and an aspect ratio of about 5. SiC particles are single crystals of equivalent diameter 200 nm and approximately globular shape. Despite HP, the Si_3N_4 grains did not show any preferred orientation. The yttria reacts during densification with the silica (which coats α-Si_3N_4 particles) and forms a liquid which solidifies at the grain boundaries. This grain boundary phase can be found in the form of thin films on grain junctions and in triple-point pockets.

5. Calibration

Calibration was demonstrated by comparing measured diffusivity values with 'Standard Reference Materials' (SRMs) of the US National Institute of Standards and Technology (NIST). SRMs are monolithic materials and the only issue concerning using them for calibrating the PD method is the extent to which high enough frequencies can be used to make them thermally thick, while at the same time maintaining good signal-to-noise ratio for accurate measurement of the beam-bending components. We have previously shown (Chung *et al.* 1997) that NIST values are reproduced to within 5%.

Here we again discuss calibration and, additionally, the effect of frequency on penetration depth. For this purpose, we select a material that is itself a composite with a 'high' thermal diffusivity, a 'small' thickness, and for which an independent measurement of thermal diffusivity has been reported. A mixture of 85% (wt) tungsten and 15% (wt) copper (as a filler) which is a 1 mm thick plate, satisfies these requirements. An independent measurement of thermal diffusivity for this material was reported by Taylor *et al.* (1995). The variation of $\mathrm{Re}(M_{\tan})$ with x was measured over a range of frequencies and the results used to obtain the dependence of χ_0 on frequency.

Figure 5 shows a typical variation of $\mathrm{Re}(M_{\tan})$ with x for $f = 15\,470$ Hz. Figure 5*b* is an enlargement of the region around $x = 0$, which shows how χ_0 is determined from these data. For distances sufficiently far from the origin, $\mathrm{Re}(M_{\tan}) \to 0$ as $x \to \pm\infty$ because the thermal field decays away from the heated spot. Since the reduction of $\mathrm{Re}(M_{\tan})$ generally occurs close to χ_0 for virtually all the materials we studied, χ_0 is a useful if not direct measure of the thermal penetration depth. As shown in figure 5, for $f = 15\,470$ Hz, $\chi_0 \approx 0.1$ mm. Since $\Delta_s = 1$ mm for this sample, the material is thermally thick at this frequency.

A cross-plot of χ_0 with $f^{-1/2}$ from data similar to those shown in figure 5 at each frequency is given in figure 6. The linear variation of χ_0 with $f^{-1/2}$ is evident. Of particular interest is the range $f < 280$ Hz ($f^{-1/2} > 0.06 s^{-1/2}$), where $\chi_0 > 1$ mm. In this range, the copper–tungsten sheet is no longer thermally thick because the thermal wave is within the gas, $\chi_0 > 1$ mm. The change in m (equation (2.8)) shows the influence of air properties on temperature distribution in the solid when $\chi_0 > 1$ mm. Using equations (2.7) and (2.8) for the data in figure 6, where $f^{-1/2} < 0.06 s^{-1/2}$, gives $\alpha_{\mathrm{copper-tungsten}} \approx 57.5\ \mathrm{mm^2\ s^{-1}}$. This value is within 3% of that reported by Taylor *et al.* (1995) for the same material.

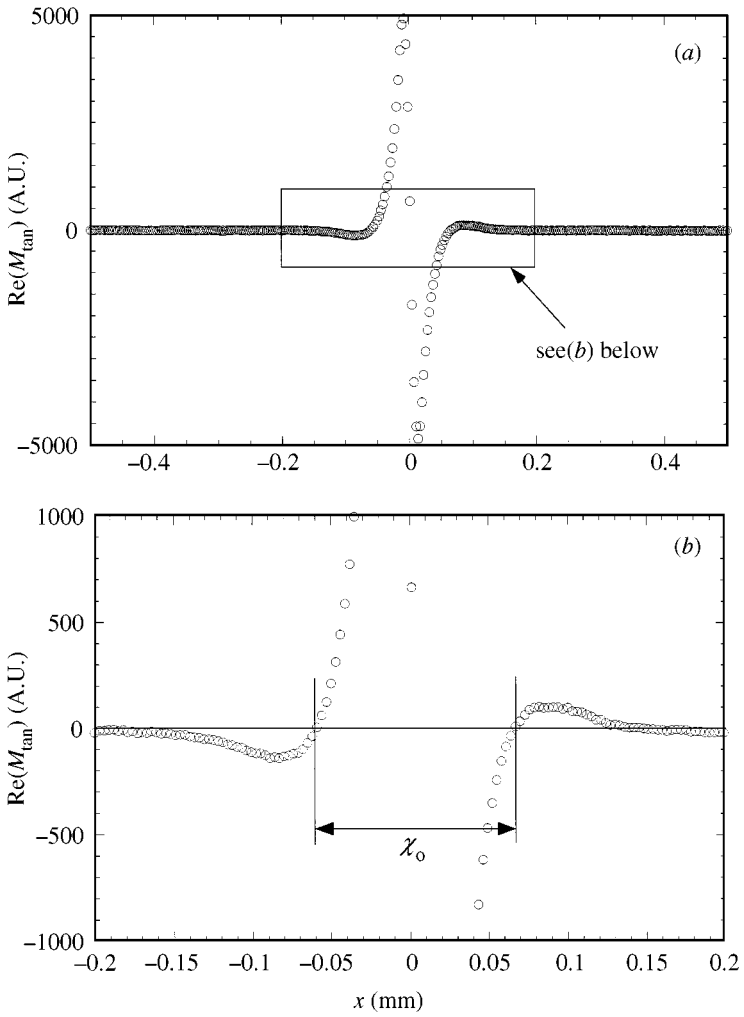

Figure 5. (*a*) Typical variation of $\mathrm{Re}(M_{\tan})$ with x for the tungsten–copper composite ($f = 15\,470$ Hz). (*b*) Enlargement of (*a*) showing how χ_0 is determined.

Since the PD technique is based on establishing a steady periodic temperature distribution in the solid by laser heating, it is necessary to keep the sample surface close to the ambient (room) temperature so that a meaningful temperature can be assigned to thermal diffusivity. Alternatively, the region enclosed by the dotted line in figure 3 could be placed in a thermally controlled atmosphere (which here was our laboratory room). At the same time, the signal-to-noise ratio must be high to maintain accuracy. For the data reported here, the argon–ion laser-beam power was 30 mW and a beam waste of beam 13.0 μm was used, which produced an acceptable signal-to-noise ratio. To estimate surface temperature for these conditions a worst case is heating a spot on the (assumed semi-infinite) solid and no heat transfer to the gas. This situation is a simple problem in conduction-shape factor algebra. For our composites our lowest measured thermal diffusivity is $16.56\ \mathrm{mm^2\ s^{-1}}$ at $\Phi = 0.30$ (table 1). Expressing ρC_p by a rule of mixtures (Chamis 1987) and using prop-

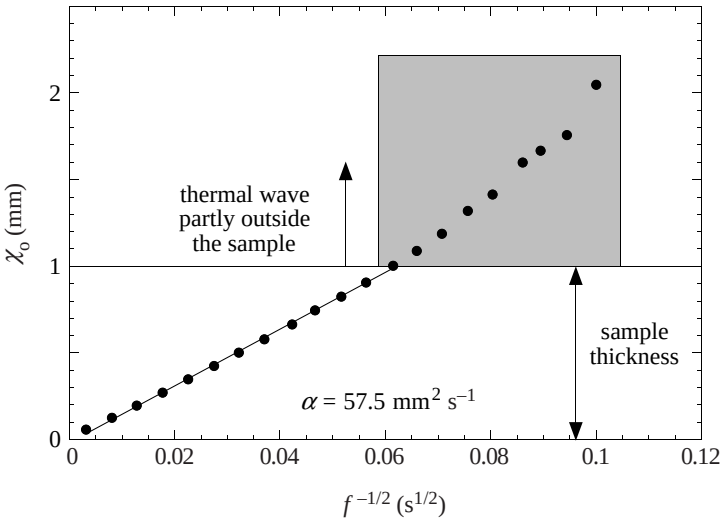

Figure 6. Cross-plot of χ_0 with $f^{-1/2}$ for the tungsten–copper composite.

Table 1. *Thermal diffusivity of* Si_3N_4/SiC *composites*
(SiC mean particle size is 200 nm. 0.08% wt fraction Y_2O_3 used as sintering aid.)

weight fraction SiC	thermal diffusivity ($mm^2\ s^{-1}$)
0.05	18.78 ± 0.22
0.10	27.87 ± 7.19
0.15	17.32 ± 0.18
0.25	16.70 ± 0.11
0.30	16.56 ± 0.16

erties from Incropera & DeWitt (1990), Lide (1991) and Touloukian *et al.* (1973) ($\rho_{Si_3N_4} \approx 3440\ kg\ m^{-3}$, $\rho_{SiC} \approx 3217\ kg\ m^{-3}$, $\rho_{Y_2O_3} \approx 5010\ kg\ m^{-3}$, $(C_p)_{Si_3N_4} \approx 691\ J\ kg^{-1}\ K^{-1}$, $(C_p)_{SiC} \approx 675\ J\ kg^{-1}\ K^{-1}$ and $(C_p)_{Y_2O_3} \approx 455\ J\ kg^{-1}\ K^{-1}$) gives $(\rho C_p)_{composite,30\%} \approx 2.31 \times 10^6\ J\ kg^{-1}\ K^{-1}$, whereby the composite thermal conductivity is predicted to be $30\ W\ m^{-1}\ K^{-1}$. Then, since $q = SK\Delta T$ where $S = 4R_1$ (Incropera & DeWitt 1990), for $q = 30$ mW, $R_1 \approx 13\ \mu m$ and $\kappa = 38\ W\ m^{-1}\ K^{-1}$ we find that $\Delta T \approx 15$ K. The NIST SRM of iron gives $\Delta T \approx 7$ K. For a square-wave modulated beam in which the period is half of the duty cycle, which is the approximate situation for the AO modulator we used, these estimates drop by a factor of two. Thus, the temperature to which we assign our measured diffusivity values is within *ca.* 20 °C of room temperature. We do not expect a significant change in the composite thermal diffusivity values we report between room temperature and 320 K.

This predicted small temperature increase of the test surface makes the neglect of convection in the gas phase a reasonable assumption. This question was previously addressed by Chung (1995) in which the effects of natural convection were estimated by measuring $\mathrm{Re}(M_{\tan})$ values for vertically oriented materials with thermal diffusivities that were lower than SiC and Si_3N_4 and which, therefore, will show a

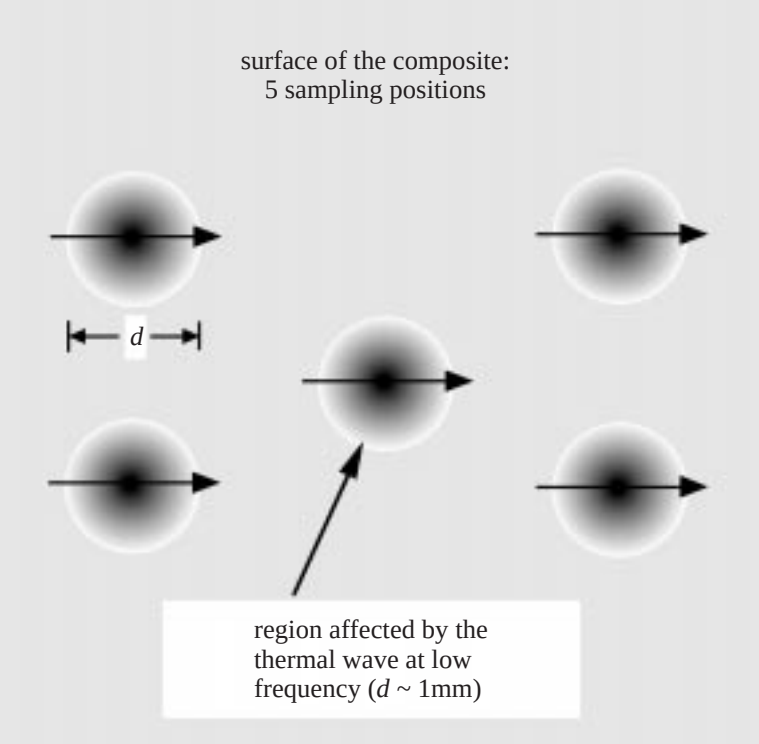

Figure 7. A map of five sampling locations for the thermal diffusivity measurements of SiC/Si_3N_4 composites. The arrows show the direction of scanning.

larger temperature difference between the surface and ambient air than the composite constituents examined here. For heating-beam powers above 500 mW, significant asymmetries in the variation of $\mathrm{Re}(M_{\tan})$ with x (which was aligned with the gravity vector) were measured, thus showing the effect of natural convection. For smaller beam powers, such as those used in this study (30 mW), natural convection will be entirely negligible, thus validating the assumption made in § 2 for the test conditions examined.

6. Results

Scans of $\mathrm{Re}(M_{\tan})$ with x (figure 1*a*) were measured for each sample five times, one time each at the five locations schematically illustrated in figure 7. The shading in figure 7 schematically illustrates the thermal penetration depth extending from the heated spot located at $x = y = z = 0$. It encompasses a statistically significant region such that the thermal diffusivity is an average over the extent of the penetration depth. A sixth scan was made for each sample at one of the five locations previously scanned under the same experimental conditions, but without moving the sample from its mount and without realigning the optical set-up. Furthermore, the $\Phi = 0.30$ composite was probed with the laser beam, heating a spot on a plane perpendicular to the usual plane of testing to examine the extent of material isotropy. The result showed an average zero-crossing slope, m in equation (2.8), in the perpendicular plane that agreed with the values of m obtained using the primary testing orientation.

To determine thermal diffusivity from measured values of m requires that b in equation (2.8) be known. As remarked earlier, b depends on the absorption coefficient of the material, σ, and such data are not available for the SiC/Si_3N_4 composites we fabricated. In an effort to establish how σ (and hence b) might depend on composition, we measured the reflectivity for the composites by the 'optical reflection method' (Jackson 1975; Herman 1996) in which the reflectivity is related to absorption coefficient. We carried out the reflection experiments using laser light at 514 nm polarized in mutually orthogonal orientations, s and p, for rotation angles between 5° and 50° in increments of 2°. The results were analysed using formulations developed by Fahrenfort & Visser (1962). We found that the absorption coefficient for the five compositions examined was greater than $10^6\ m^{-1}$. Such a large value is indicative of an absorbing material. This value corresponds to optical penetration depths of less than 1 μm, which is much lower than the smallest thermal penetration depth created by the highest modulation frequency used (2000 Hz). According to the analysis of Salazar *et al*. (1989), such a large absorption coefficient will be in an asymptotic range where a single value of b characterizes the material. The formulations listed in § 2 result in $b \approx 1.2$ for such materials, which is the 'point absorption' value. This is the value used in equation (2.8) to obtain thermal diffusivity from measured values of m.

Table 1 lists values of α using equation (2.8) and $b \approx 1.2$, and figure 8*a* displays graphically the variation of α with composition. In figure 8*a* an average of five measurements made on each sample (figure 7) is shown. Table 1 also lists the standard deviations of α for each composition. The largest standard deviation is for the 10% composite, which also shows the highest average thermal diffusivity. For all but the 0.10 composition, error bars shown in figure 8*a* would be less than the size of the data symbols. Therefore, only the error bar for the 0.10 composition is shown in figure 8*a*.

The effect of a high SiC thermal diffusivity and small SiC particle size (which increases the particle–matrix surface-to-volume ratio and the total thermal contact resistance) compete to produce a maximum thermal diffusivity at $\Phi = 0.10$. Other material properties have also shown extrema for Si_3N_4/SiC composites at the same weight fraction. One in particular—fracture toughness—has been found to show a maximum at $\Phi = 0.10$ (Sawaguchi *et al*. 1991). Interestingly, the largest standard deviation of fracture toughness was measured for $\Phi = 0.10$ from among the samples tested by Sawaguchi *et al*. (1991). The composites studied were similar to ones we examined except that 6% (wt) Y_2O_3 and 2% (wt) Al_2O_3 were used as a binder, whereas we used 8% (wt) Y_2O_3 in the present study. Another property—creep rate—shows a minimum at $\Phi = 0.10$ for composites identical to those examined here (Rendtel *et al*. 1997; Rendtel & Hübner 1996).

The increased scatter of thermal diffusivity at $\Phi = 0.10$ relative to the other compositions studied is evidenced by the raw data for χ_0 shown in figure 9 for $\Phi = 0.10$ and 0.15. Data from the five measurement locations (see figure 7) are shown. It is clear from figure 9*a* that the scatter in χ_0 is considerable for $\Phi = 0.10$ for scan 5 relative to the other compositions (and also for the other locations on the 10% composite). The microstructures shown in figure 4 do not offer obvious clues. Several prior studies (i.e. Pezzotti & Sakai 1994; Niihara *et al*. 1989; Niihara 1991; Sasaki *et al*. 1992; Hirano *et al*. 1994; Rouxel *et al*. 1992) have, however, reported that the grain shape of Si_3N_4 appears to transform from an elongated to a globular shape at weight fractions slightly over 0.10.

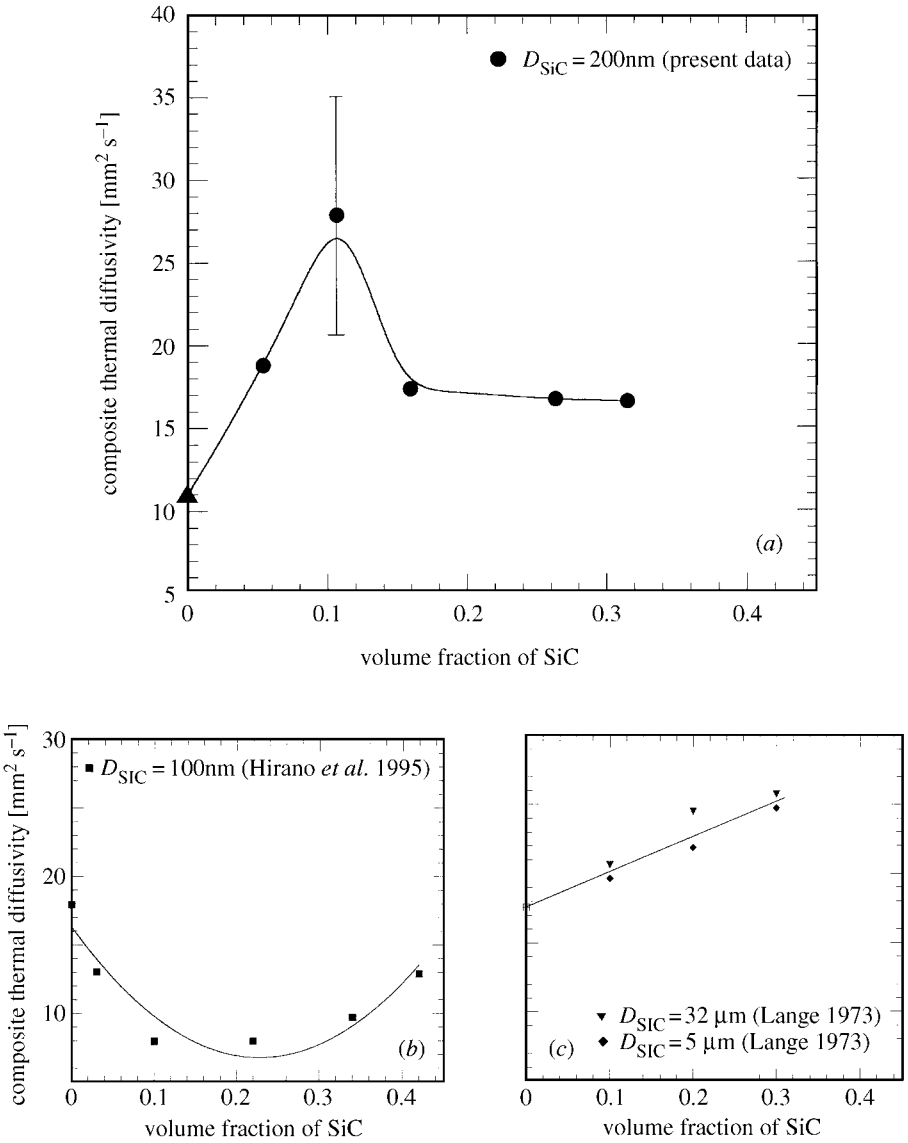

Figure 8. Variation of the mean thermal diffusivity with ϕ for SiC/Si_3N_4 composites: (*a*) present data; the data at $\phi = 0$ come from Tsukuma *et al.* (1981); (*b*) Hirano *et al.* (1995); (*c*) Lange (1973).

Also illustrated in figure 8 are the measurements of Lange (1973) and Hirano *et al.* (1995) that show the differing trends with SiC concentration. The data at $\Phi = 0$ in figure 8*a* come from Tsukuma *et al.* (1981) who report the thermal diffusivity for Si_3N_4 with 4% of Y_2O_3 and a grain size of a few microns. The monotonic increase of Lange's data is clearly evident as is the minimum measured by Hirano *et al.* (1995). The smaller 100 nm particles used by Hirano *et al.* (1995) result in an immediate controlling influence of interfaces for $\Phi > 0$, which presumably would give way to the high SiC thermal conductivity as $\Phi \to 1$.

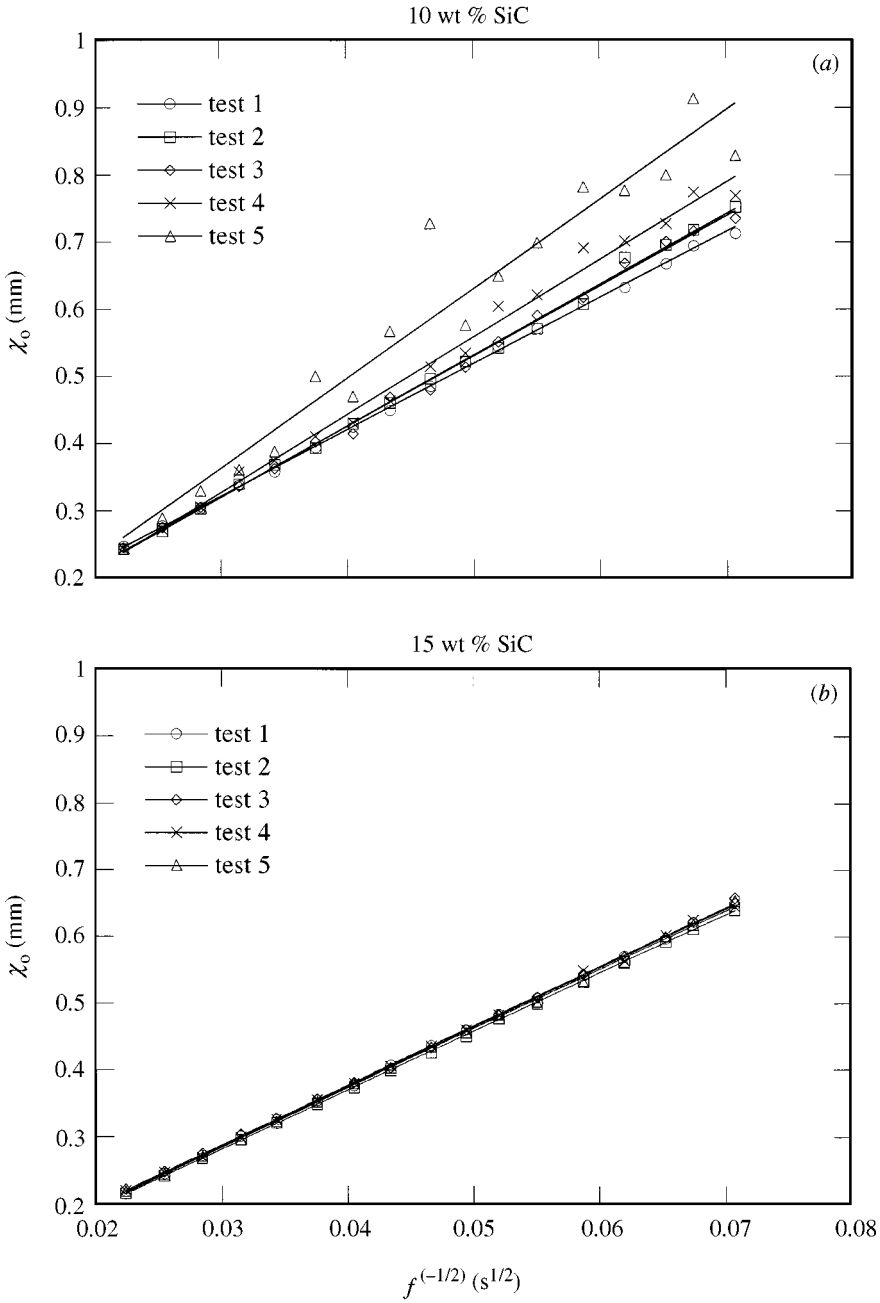

Figure 9. Variation of χ_0 with $f^{-1/2}$ for the sample containing (*a*) $\Phi = 0.10$; (*b*) $\Phi = 0.15$ of SiC.

As to the role of the binder, it concentrates as a film at the SiC/Si_3N_4 interface and at the SiC/Si_3N_4 boundary and can effect the thermal contact resistance. As noted by Rendtel *et al*. (1997), for 'larger' SiC particles the interface between SiC particles and an Si_3N_4 matrix contains an amorphous layer of products of reaction between

Y_2O_3, silica, impurities, SiC and Si_3N_4. On the other hand, 'small' SiC particles are usually directly bonded to Si_3N_4 and occupy intragranular locations. As Φ varies, the thickness of the binder and the interface microstructure could conceivably change. Impurities introduced into the composites during preparation or through the powder can also play a role. The variability of these influences as Φ changes complicates attributing specific trends of the composite thermal diffusivity to any one of them.

Equation (1.1) and alternative forms which rigorously include terms up to ϕ^2 (see, for example, Jeffrey 1973; Felderhof *et al*. 1982) or consider multicomponent composites with coated dispersed particles (Dunn & Taya 1993) all assume that the microstructure of the constituents and interfaces does not change with particle size and concentration. Simple closed-form solutions are derived by Chiew & Glandt (1987) that include the effect of the particle–matrix thermal-contact resistance. Though derived for microstructures that do not match exactly the composites we studied, it is still useful to discuss trends from these formulations. These assumptions undoubtedly work for many composites (e.g. epoxy–metallic and some ceramic–metal composites), but apparently not for the Si_3N_4/SiC composites we studied. One obvious result from equation (1.1) is that the predicted thermal diffusivity only increases as ϕ increases, and a singularity occurs at $\phi = 1/\beta$.

To account for a finite thermal-contact resistance between the particles (assumed spherical) and surrounding matrix, Chiew & Glandt (1987) assume a zero interface thickness (no binder present) across which a temperature jump occurs due to a contact resistance. A modified closed-form expression for β in equation (1.1) is

$$\beta = \frac{\varepsilon - R_c - 1}{\varepsilon + 2(R_c + 1)}, \tag{6.1}$$

where R_c is a non-dimensional thermal-contact resistance ($\equiv R_{tc}\kappa_p/D$, where R_{tc} ($m^2\ K^{-1}\ W^{-1}$) is the dimensional contact resistance between the particle of effective diameter D and surrounding matrix). R_c ranges from 0 to ∞, but β should be independent of ϕ according to equation (6.1). A 'perfect' interface is one for which $R_{tc} = 0$ (equation (1.2)). Though R_c is unknown, we arbitrarily varied it from 0 to ∞ in order to obtain bounds on β. For the Si_3N_4/SiC composite system $\varepsilon \approx 9$, and equation (6.1) shows that $-0.5 < \beta < 0.73$. We compared this range with values of β obtained by inverting equation (1.1) using the four measurements of table 1. The results show that only for $\Phi > 0.10$ are the values of β in the predicted range and that, furthermore, there is a clear dependence of β on ϕ for all compositions, contrary to what is assumed in the models.

Two possible reasons for the failure of this model for Si_3N_4/SiC composites are that (a) the model was formed for binary mixtures, but our composites are in fact ternary mixtures; and (b) the potential for the aforementioned dependence of R_c on ϕ, as that is the only way β could change as ϕ is varied. For example, taking R_c to vary linearly with ϕ we found qualitatively that a maximum of thermal diffusivity is predicted by equation (6.1) in equation (1.1). However, there is poor quantitative agreement both for our measurements and for those of others. And it is unlikely that other properties, for example specific heat and density, are influenced by composition in a way that could produce an extrema of thermal diffusivity with composition.

Effects that need to be better understood for modelling include imperfections in the Si_3N_4 matrix grains, which can impede heat flow; thermal expansion mismatch between SiC and Si_3N_4; distortions created by SiC particles in the Si_3N_4 matrix; and

the effect of the sintering aid on the microstructure. Future work should, therefore, seek to better characterize the role of SiC particle loading, size (and shape) and binder on microstructure from which a predictive formulation for thermal diffusivity may emerge for this composite.

This work was supported by the Semiconductor Research Corporation (Dr Ron C. Bracken, project monitor) and the Industry-Cornell Alliance for Electronic Packaging (Dr Che-Yu Li, project monitor). A.P.C. was partly supported by the Zonta International Foundation through an Amelia Earhart Fellowship. We thank Mr Yoke Chung of Intel Corporation, Dr Roger Schmidt of IBM (Poughkeepsie), Dr Grady White of NIST, Professor Rishi Raj (University of Colorado), Professor Sievers and his colleagues (Cornell), Professor Che-Yu Li (Cornell) and Professor Simon Bauer (Cornell) for many helpful discussions throughout the course of our work. We also thank Dr Frank Pompeo and Dr Raed Sherif of IBM (East Fishkill) for providing the copper–tungsten composite and information related to prior measurements for it, and the Fraunhofer Institute of Ceramic Technologies and Sintered Materials at Dresden, Germany, for fabrication of the materials.

Nomenclature

Symbols not defined in the text or symbols that are often used.

C_p	specific heat
c	constant
f	modulation frequency of the heating beam
h	height of probe beam
i	imaginary number
$\mathrm{Im}(M_{\tan})$	imaginary part of tangential deflection
k	Fourier transform variable
n	index of refraction
n_0	index of refraction of ambiance
$R_{1,2}$	radius of the heating or probe beam, respectively
$\mathrm{Re}(M_{\tan})$	real part of tangential deflection
t	time
T	temperature
x, y, z	spatial coordinates defined in figure 1
α	thermal diffusivity
χ_0	zero crossing (see figure 5)
ε	particle-to-matrix conductivity ratio
κ	thermal conductivity
Δ	film thickness
ϕ	volume fraction of the SiC particles in the composite
Φ	mass fraction of the SiC particles in the composite
ρ	density

Subscripts

g	gas
f	film
s	substrate
c	composite
m	matrix
p	particle

References

Arpaci, V. S. 1966 *Conduction heat transfer*, ch. 6. Reading, MA: Addison-Wesley.

Bhatt, H., Donaldson, K. Y. & Hasselman, D. P. H. 1990 *J. Am. Ceram. Soc.* **73**, 312.

Bigg, D. M. 1986 *Poly. Comp.* **7**, 125–140.

Buljan, S. T., Baldoni, G. J. & Huckabee, M. L. 1987 *Am. Ceram. Soc. Bull.* **66**, 347.

Chamis, C. C. 1987 in *Engineering guide to composite materials* (ed. J. Weeton *et al.*), 3-8–3-24. Materials Park, OH: ASM International.

Chiew, Y. C. & Glandt, E. D. 1987 *Chem. Engng Sci.* **42**, 2677.

Chung, Y. D. 1995 MS thesis, Department of Mechanical and Aerospace Engineering, Cornell University, USA.

Chung, Y. D., Chojnacka, A. P., Avedisian, C. T. & Raj, R. 1997 *Acta Mater.* **45**, 2983–2993.

Dunn, M. L. & Taya, M. 1993 *J. Appl. Phys.* **73**, 1771–1722.

Evans, A. G. 1995 *Phil. Trans. R. Soc. Lond.* A **351**, 511–527.

Fahrenfort, J. & Visser, W. M. 1962 *Sectrochim. Acta* **18**, 1103–1116.

Felderhof, B. U., Ford, G. W. & Cohen, E. G. D. 1982 *J. Stat. Phys.* **28**, 649–672.

Gibiansky, L. V. & Torquato, S. 1996 *Proc. R. Soc. Lond.* A **452**, 253–283.

Graebner, J. E. 1993 *Diamond Films Technol.* **3**, 77.

Hasselman, D. P. H & Johnson, L. F. 1987 *J. Compos. Mater.* **21**, 508.

Herman, I. P. 1996 *Optical diagnostics for thin film processing*, pp. 328–335. Boston, MA: Academic.

Hermel, W., Herrmann, M., Schubert, C., Klemm, H., Millers, T. & Rendtel, A. 1994 In *Int. Conf. Structure and Properties of Brittle and Quasiplastic Materials.* pp. 21–25. Riga, Latvia.

Herrmann, M., Millers, T., Rendtel, A., Reich, T., Boden, G. & Schubert, C. 1993 In *Engineering ceramics* (ed. P. Duran & J. F. Fernandez) (3rd Euro-ceramics, vol. 3), pp. 603–607. Madrid: Faenza Editrice Iberica.

Herrmann, M., Schubert, C., Rendtel, A. & Hübner, H. 1997 *J. Am. Ceram. Soc.* **81**, 1095–1108.

Hirano, T., Nakahira, A. & Niihara, K. 1994 *J. Jap. Soc. Powder Powder Metall.* **41**, 1243–1248.

Hirano, T., Izaki, K. & Niihara, K. 1995 *Nanostruct. Mater.* **5**, 809.

Incropera, F. & DeWitt, F. 1990 *Introduction to heat transfer*, 2nd edn. New York: Wiley.

Jackson, J. D. 1975 *Classical electrodynamics*, 2nd edn, pp. 278–282. New York: Wiley.

Jeffrey, D. J. 1973 *Proc. R. Soc. Lond.* A **335**, 355–367.

Kelly, A. 1996 *Phil. Trans. R. Soc. Lond.* A **354**, 1841–1874.

Lange, F. F. 1973 *J. Am. Ceram. Soc.* **56**, 445.

Lide, D. R. (ed.) 1991 *CRC handbook of chemistry and physics*, 72nd edn, pp. 4–95. Boca Raton, FL: CRC.

Maxwell, J. C. 1873 *Electricity and magneticism.* Oxford: Clarendon.

Nguyen, T. & Avedisian, C. T. 1994 Cornell Energy Report No. E-94-03, Sibley School of Mechanical and Aerospace Engineering, Cornell University.

Niihara, K. 1991 *J. Ceram. Soc. Jap.* **99**, 974–982.

Niihara, K., Hirano, T., Nakahira, A., Suganuma, K., Izaki, K. & Kawakami, T. 1989 *J. Jap. Soc. Powder Powder Metall.* **36**, 243. (In Japanese.)

Palchevskis, E., Grabis, J. & Millers, T. 1993 In *Proc. Pulvermetall. Tagung*, pp. 657–662. Oberursel, Dresden: DGM Informationsges.

Pezzotti, G. & Sakai, M. 1994 *J. Am. Ceram. Soc.* **77**, 3039–3041.

Rendtel, A. & Hübner, H. 1996 *Ceram. Trans.* **74**, 523–534.

Rendtel, A., Hübner, H., Herrmann, M. & Schubert, C. 1997 *J. Am. Ceram. Soc.* **81**, 1109–1120.

Reyes, C. 1988 PhD thesis, Department of Physics, Wayne State University, USA.

Reyes, C. B., Jaarinen, J., Fabro, L. D., Kuo, P. K. & Thomas, R. L. 1987 *Rev. Prog. Quant. Nondest. Eval.* **6**, 271–275.

Rouxel, T., Wakai, F. & Izaki, K. 1992 *J. Am. Ceram. Soc.* **75**, 2363–2372.

Salazar, A., Sanchez-Lavega, A. & Fernandez, J. 1989 *J. Appl. Phys.* **65**, 4150.

Salazar, A., Sanchez-Lavega, A. & Fernandez, J. 1991 *J. Appl. Phys.* **69**, 1216.

Sasaki, G., Nakase, H., Suganuma, K., Fujita, T. & Niihara, K. 1992 *J. Ceram. Soc. Jap.* **100**, 536–540.

Sawaguchi, A., Toda, K. & Niihara, K. 1991 *J. Am. Ceram. Soc.* **74**, 1142–1144.

Shalek, P. D., Petrovic, J. J., Hurley, G. F. & Gac, F. D. 1986 *Am. Ceram. Soc. Bull.* **65**, 351.

Suzuki, H. 1987 *Phil. Trans. R. Soc. Lond.* A **322**, 465–478.

Taylor, R. E., Groot, H. & Ferrier, J. 1995 Thermophysical Properties Research Laboratory—a report to IBM, no. TPRL 1496. School of Mechanical Engineering, Purdue University, West Lafayette, Indiana.

Torti, M. L., Alliegro, R. A., Richerson, D. W., Washburn, M. E. & Weaver, G. Q. 1973 *Proc. Br. Ceram. Soc.* **22**, 129.

Touloukian, Y. S., Powell, R. W., Ho, C. Y. & Nicolaou, M. C. 1973 *Thermophys. Properties Matter Thermal Diffusiv.* **10**, 407.

Tsukuma, K., Shimada, M. & Koizumi, M. 1981 *Ceram. Bull.* **60**, 910–912.

Tummala, R. R. & Rymaszewski, E. J. 1989 *Handbook of electronic packaging*, p. 36. New York: Van Nostrand Reinhold.

Wei, G. C. & Becher, P. F. 1985 *Am. Ceram. Soc. Bull.* **64**, 298.

Wei, L. 1993 PhD thesis, Department of Physics, Wayne State University, USA.

Wei, L., Vaudin, M., Hwang, C. S. & White, G. 1995 *J. Mater. Res.* **10**, 1889.

Weiderhorn, S. M. & Tighe, N. J. 1983 *J. Am. Ceram. Soc.* **66**, 884.

Zdaniewski, W., Hasselman, D. P. H., Knoch, H. & Heinrich, J. 1979 *Am. Ceram. Soc. Bull.* **58**, 539.